Hyperfine Interact (2016) 237: 136
DOI 10.1007/s10751-016-1340-3

Composition of $\alpha - Fe$ nanoparticles precipitated from CuFe alloy studied by hyperfine interactions

Denisa Kubániová[1] · Martin Cesnek[2] · Ondrej Milkovič[3] · Jaroslav Kohout[1] · Marcel Miglierini[2]

Published online: 27 September 2016

Abstract Iron-based nanoparticles prepared by precipitation from solid solution of saturated binary Cu-Fe alloy were studied by transmission electron microscopy, high-energy X-ray diffraction and Mössbauer spectroscopy. The results showed that the investigated as-prepared nanoparticles contained two phases. The major phase was determined as $\alpha - Fe$ and the minor phase as $\gamma - Fe_2O_3$. Furthermore, additionally annealed samples in Ar protective atmosphere were investigated. Results showed clear decrease in contribution of $\alpha - Fe$ phase and also revealed the presence of various iron oxides (maghemite, magnetite, hematite and wűstite).

Keywords Iron-based · Nanoparticles · Precipitation

1 Introduction

Iron-based magnetic nanoparticles have been recently intensively studied due to their valuable features in comparison with bulk materials. Such nanoparticles in contrast with the

This article is part of the Topical Collection on *Proceedings of the International Conference on Hyperfine Interactions and their Applications (HYPERFINE 2016), Leuven, Belgium, 3-8 July 2016*

✉ Martin Cesnek
martin.cesnek@fjfi.cvut.cz

Denisa Kubániová
kubaniova@mbox.troja.mff.cuni.cz

[1] Faculty of Mathematics and Physics, Charles University, V Holesovickach 2, 180 00 Prague, Czech Republic

[2] Department of Nuclear Reactors, Czech Technical University, V Holesovickach 2, 180 00 Prague, Czech Republic

[3] Institute of Materials Research, Slovak Academy of Sciences, Watsonova 47, 040 01 Kosice, Slovak Republic

other types of nanoparticles have many advantages such as superior environmental compatibility, low cost, biocompatibility and high magnetic saturation [1–3]. Thus they have a wide variety of promising applications such as water treatment, environmental remediation, biomedicine, etc. [4–6]. As it was reported earlier in [7, 8], an advantage of $\alpha - Fe$ nanoparticles over Fe_3O_4 or Fe_2O_3 nanoparticles might be their higher saturation magnetization.

Iron-based nanoparticles can be prepared by a wide variety of methods. This paper focuses on nanoparticles prepared by a method which uses precipitation in solid state. The precipitants are afterwards obtained by chemical or electrochemical dissolution of matrix. As-prepared $\alpha - Fe$ nanoparticles are unstable and rapidly oxidize what leads to a core-shell structure of nanoparticles [9]. The core of nanoparticles consists of $\alpha - Fe$, which creates body centered cubic lattice with the lattice parameter 2.86 Å at room temperature [10] and it is ferromagnetically ordered up to 768 $^{\circ}C$ [11]. The shell surrounding the $\alpha - Fe$ core is formed by the thin layer of iron oxide which protects the core against further oxidation. It was reported in [12–15] that the shell of such nanoparticles might consist of iron oxides as maghemite or magnetite. It should be noted that due to very close cell parameters and small oxide layer thickness, it is very difficult to distinguish between magnetite and maghemite using diffraction techniques [13, 16].

As it was showed earlier in [17–20] Mössbauer spectroscopy (MS) seems to be suitable tool for investigation of such samples. This method enables to relatively precisely distinguish between different forms of iron oxides. The aim of this paper is to determine the core-shell structure of iron nanoparticles and identify kinds of iron oxides in shell of the iron-based nanoparticles prepared by the mentioned method.

2 Samples and methods

Investigated iron based nanoparticles were prepared by precipitation from solid solution of saturated binary $Cu - Fe$ alloy with 1.25 wt.% which was annealed at 973 K for 18 hours. Nanoparticles were subsequently isolated by dissolution of Cu matrix. The annealed $Cu - Fe$ alloy is dissolved in $NH_4OH + H_2O_2$ solution. The process of the preparation is described in more detail in [21]. Moreover, studied nanoparticles were additionally annealed at $853K$ in Ar protective atmosphere. Size distribution of nanoparticles was checked by transmission electron microscopy (TEM). All the TEM images were obtained by transmission electron microscope JEOL JEM-2000FX operated at $200kV$. Furthermore, the structure was analyzed by high-energy x-ray diffraction (HEXRD) and MS. MS spectra were recorded in transmission geometry using constant acceleration spectrometer with a $^{57}Co/Rh$ source. MS spectra of non-annealed sample were recorded at room temperature (RT) and at $4.2K$ using a liquid helium bath cryostat. MS spectrum of additionally annealed sample was recorded so far only at RT . All the resulting isomer shifts are quoted relative to the MS spectrum of a 12.5 μm thin bcc-Fe foil recorded at RT. The spectral parameters comprising isomer shift (IS), quadrupole splitting/quadrupole shift (QS), hyperfine magnetic field (B), line width (Γ), and area (A) of spectral components were refined by the CONFIT curve-fitting program [22]. HEXRD experiment was done at the PETRA III storage ring at DESY (Hamburg, Germany). The sample was irradiated by a photon beam with the size of 0.5 × 0.5 mm^2 and energy of 60 keV (λ = 0.20727 Å) for 10 s. Scattered photons were recorded with 2D detector (Perkin Elmer 1621, 2048 × 2048 pixels, pixel size 200 × 200 mm^2). The raw HEXRD patterns were radially integrated with help of Fit2D [23].

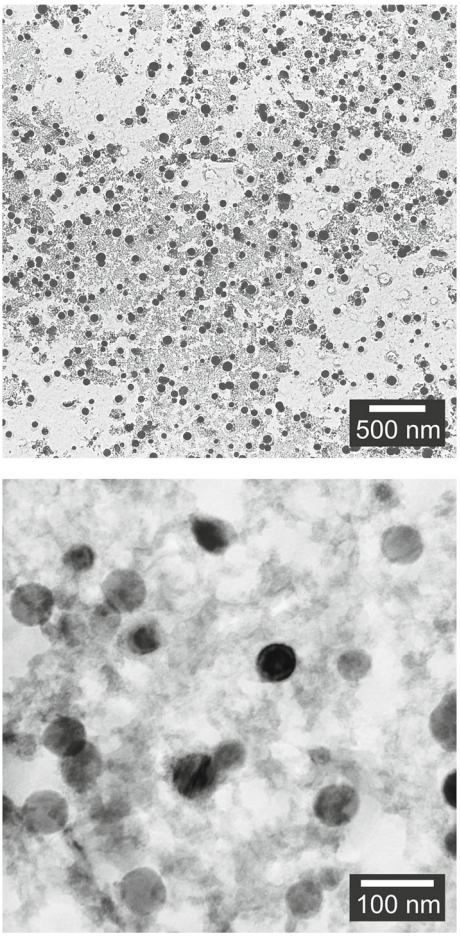

Fig. 1 TEM images of studied nanoparticles

3 Results and discussion

TEM images of the non-annealed nanoparticles in the powder form are shown in Fig. 1. Cores of the nanoparticles are represented by dark traces and shells are shown by lighter traces in the TEM images. The mean size of the nanoparticles is 54 nm and the particle size distribution itself can be seen in Fig. 2. The shape of the particle size distribution evinces negative inclination (extreme value distributions) typical for nanoparticles produced in magnetotactic bacteria [24, 25] unlike log-nornal distributions typical for synthetic nanoparticles e.g. $\epsilon - Fe_2O_3$ [26]. It can be seen that studied non-annealed nanoparticles with relatively large mean size prepared by method discussed earlier exhibit wide particle size distribution.

Radially integrated HEXRD diffraction pattern is shown in Fig. 3. These data reveal one major crystalline phase and at least one minor phase. The major crystalline phase was clearly identified as $\alpha - Fe$ and might form the core of nanoparticles. The minor phase exhibits structural disorder which is indicated by broadened peaks and might form the shell of nanoparticles. Although it was not possible to precisely identify this phase it might correspond to $CuFe_2O_4$, Fe_3O_4 or $\gamma - Fe_2O_3$.

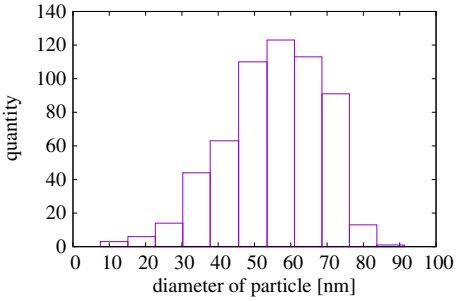

Fig. 2 Distribution of particle sizes

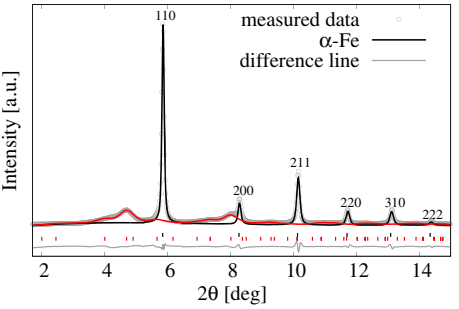

Fig. 3 Radially integrated HEXRD pattern. The red line represents unspecified minor phase

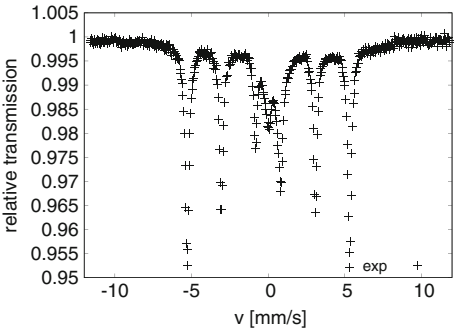

Fig. 4 MS spectrum of non-annealed sample obtained at RT

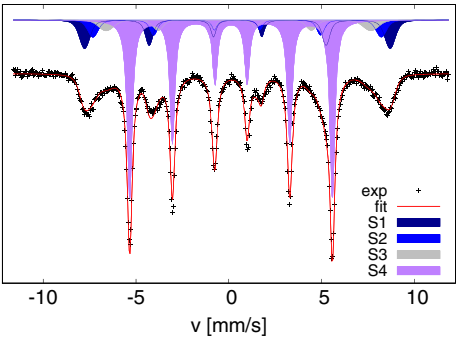

Fig. 5 MS spectrum of non-annealed sample obtained at 4 K

Table 1 Hyperfine parameters of spectral components of non-annealed sample measured at 4.2 K

		IS [mm/s] (± 0.02 mm/s)	QS [mm/s] (± 0.02 mm/s)	Bhf [T] (± 0.5 T)	A [%] (± 1 %)
S1	$\gamma - Fe_2O_3$ octahedral	0.47	−0.01	51.1	17
S2	$\gamma - Fe_2O_3$ tetrahedral	0.45	0.00	48.2	11
S3	-	0.42	0.21	44.3	9
S4	$\alpha - Fe$	0.12	0.00	33.9	63

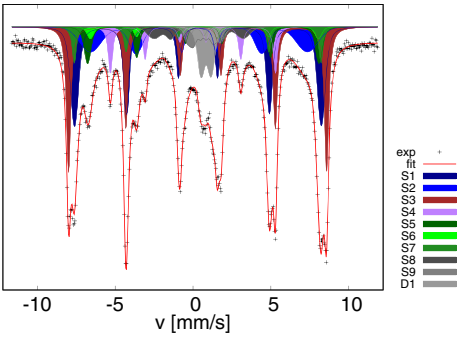

Fig. 6 MS spectrum of annealed sample obtained at RT

Table 2 Hyperfine parameters of spectral components of annealed sample measured at RT

		IS [mm/s] (± 0.02 mm/s)	QS [mm/s] (± 0.02 mm/s)	Bhf [T] (± 0.5 T)	A [%] (± 1 %)
S1	$\gamma - Fe_2O_3$ octahedral	0.32	0.00	49.2	25
S2	$\gamma - Fe_2O_3$ tetrahedral	0.38	0.00	43.3	15
S3	$\alpha - Fe_2O_3$	0.39	−0.19	51.4	23
S4	$\alpha - Fe$	0.00	0.00	32.9	7
S5	Fe_3O_4 octahedral	0.67	−0.03	46.1	8
S6	Fe_3O_4 octahedral	0.67	0.11	45.4	3
S7	Fe_3O_4 tetrahedral	0.29	0.01	49.2	6
S8	–	0.29	0.13	17.8	4
S9	–	0.70	0.07	6.7	4
D1	FeO	0.84	0.65	–	5

MS spectrum obtained at RT from non-annealed sample is shown in Fig. 4. This spectrum reveals major six-line pattern which can be assigned to $\alpha - Fe$. This fact is in good agreement with results obtained by HEXRD measurements. In addition to that superparamagnetic relaxation can be observed and unfortunately it was not possible to identify the other phases from RT spectrum. In order to obtain more information about the other possible phases present in the sample, MS spectrum was recorded at 4.2 K. Low temperature spectrum of non-annealed sample together with spectral components can be seen in Fig. 5. This spectrum reveals in addition to $\alpha - Fe$ three broadened sextets. Such broadened six-line patterns indicate structural disorder what is again in good agreement with HEXRD measurements. The hyperfine parameters (isomer shift - IS, quadrupolar shift - QS and average hyperfine magnetic field - B_{hf}) of the sextets S1 and S2 together with the ratio of their fractions 5:3 are typical for γ-polymorph of Fe_2O_3 (maghemite) [27, 28]. Broadened sextet marked as S3 might represent interface between crystalline $\alpha - Fe$ and $\gamma - Fe_2O_3$. MS spectral parameters corresponding to mentioned spectral components are listed in Table 1.

MS spectrum of additionally annealed sample obtained at RT is shown together with corresponding spectral components in Fig. 6. A significant decrease in contribution of $\alpha - Fe$ phase which corresponds to sextet S4 and growth of several iron oxides is observable. MS spectrum reveals in comparison with non-annealed sample an increase in contribution of maghemite $\gamma - Fe_2O_3$ (S1 corresponds to octahedral sites and S2 to tetrahedral sites). Furthermore, presence of new iron oxides was detected. According to hyperfine parameters sextet S3 was identified as hematite $\alpha - Fe_2O_3$ [29]. Sextets S5, S6 correspond to octahedral sites and sextet S7 represents tetrahedral sites of magnetite Fe_3O_4 [29]. Doublet D1 exhibits hyperfine parameters typical for wűstite FeO [30]. In addition to that two sextet distributions with low mean value of hyperfine magnetic field can be observed in the spectrum. One of the sextets marked as S8 can be assigned to trivalent iron. Distributed sextet S9 might suggest paramagnetic relaxation. MS spectral parameters of corresponding spectral components of annealed sample are listed in Table 2.

4 Conclusion

Samples of iron-based nanoparticles prepared by precipitation from solid solution of saturated binary Cu-Fe were investigated. Both high-energy X-ray diffraction and Mössbauer spectroscopy results reveal one major phase in the case of non-annealed sample which was with help of both methods clearly identified as $\alpha - Fe$. Furthermore, minor phase exhibiting structural disorder was observed by both methods. Mössbauer spectroscopy results suggest that this minor phase might be $\gamma - Fe_2O_3$. Moreover, additionally annealed samples were investigated. Mössbauer spectrum obtained at room temperature shows clear decrease in contribution of $\alpha - Fe$ phase, rise in contribution of $\gamma - Fe_2O_3$ and even presence of new iron oxides in comparison with non-annealed sample. The latter are probably caused by residual oxygen even though a protective atmosphere was used during the annealing.

Acknowledgment This work was supported by the grant GACR 16-04340S.

References

1. Zhang, W.: Nanoscale iron particles for environmental remediation: An overview. J. Nanopart. Res. **5**, 323–332 (2003)
2. Crane, R.A., Scott, T.B.: Nanoscale zero-valent iron: Future prospects for an emerging water treatment technology. J. Hazard. Mater. **211–212**, 112–125 (2012)

3. Cheong, S., Ferguson, P., Feindel, K.W., Hermans, I.F., Callaghan, P.T., Meyer, C., Slocombe, A., Su, Ch., Cheng, F., Yeh, Ch., Ingham, B., Toney, M.F., Tilley, R.D.: Simple synthesis and functionalization of iron nanoparticles for magnetic resonance imaging. Angew. Chem. Int. Ed. **50**, 4206–4209 (2011)
4. Tang, S.C.N., Lo, I.M.C.: Magnetic nanoparticles: Essential factors for sustainable environmental applications. Water Res. **47**, 2613–2632 (2013)
5. Curtis, A., Wilkinson, C.: Nantotechniques and approaches in biotechnology. Trends Biotechnol. **19**, 97–101 (2001)
6. Huber, D.L.: Synthesis, properties, and applications of iron nanoparticles. Small **1**, 482–501 (2005)
7. Han, Y.C., Kim, Y.H., Heo, J.K., Kang, Y.C., Kang, Y.S.: A magnetic behavior of $\alpha - Fe$ nanoparticle. NMDC **1**, 650–652 (2006)
8. Hadjipanayis, C.G., Bonder, M.J., Balakrishnan, S., Wang, X., Mao, H., Hadjipanayis, G.C.: Metallic iron nanoparticles for mri contrast enhancement and local hyperthermia. Small **4**, 1925–1929 (2008)
9. Wang, C.M., Baer, D.R., Engelhard, M.H., Amonette, J.E., Antony, J.J., Qiang, Y.: Fine structural features and electronic structure of core-shell structured Fe nanoparticles probed using TEM/STEM and EELS. Microsc. Microanal. **15**, 1204–1205 (2009)
10. Krauss, G.: Steels: Processing, Structure, and Performance. ASM International, Ohio (2005)
11. Cardarelli, F.: Materials Handbook: A Concise Desktop Reference. Springer, New York (2008)
12. Xing, L., Brink, G.H.T., Chen, B., Schmidt, F.P., Haberfehlner, G., Hofer, F., Kooi, B.J., Palasantzas, G.: Synthesis and morphology of iron-iron oxide core-shell nanoparticles produced by high pressure gas condensation. Nanotechnology **27**, 215703 (2016)
13. Signorini, L., Pasquini, L., Savini, L., Carboni, R., Boscherini, F., Bonetti, E., Giglia, A., Pedio, M.: Size-dependent oxidation in iron/iron oxide core-shell nanoparticles. Phys. Rev. B **68**, 195423 (2003)
14. Gangopadhyay, S., Hadjipanayis, G.C., Dale, B., Sorensen, C.M., Klabunde, K.J., Papaefthymiou, V., Kostikas, A.: Magnetic properties of ultrafine iron particles. Phys. Rev. B **45**, 9778 (1992)
15. Kuhn, L.T., Bojesen, A., Timmermann, L., Nielsen, M.M., Mørup, S.: Structural and magnetic properties of core-shell iron-iron oxide nanoparticles. J. Phys.: Condens. Matter **14**, 13551–13567 (2002)
16. Mikhaylova, A.B., Sirotinkin, V.P., Fedotov, M.A., Korneyev, V.P., Shamray, B.F., Kovalenko, L.V.: Quantitative determination of content of magnetite and maghemite in their mixtures by X-ray diffraction methods. Inorg. Mater. Appl. Res. **7**, 130–136 (2016)
17. Vitta, Y., Piscitelli, V., Fernandez, A., Gonzalez-Jimenez, F., Castillo, J.: $\alpha - Fe$ nanoparticles produced by laser ablation: Optical and magnetic properties. Chem. Phys. Lett. **512**, 96–98 (2011)
18. Goya, G.F., Rechenberg, H.R.: Superparamagnetic transition and local disorder in $CuFe_2O_4$ nanoparticles. Nano Struct. Mater. **10**, 1001–1011 (1998)
19. Joos, A., Rűmenapp, C., Wagner, F.E., Gleich, B.: Characterisation of iron oxide nanoparticles by Mössbauer spectroscopy at ambient temperature. J. Magn. Magn. Mater. **399**, 123–129 (2016)
20. Gabbasov, R., Polikarpov, M., Cherepanov, V., Chuev, M., Mischenko, I., Lomov, A., Wang, A., Panchenko, V.: Mössbauer, magnetization and X-ray diffraction characterization methods for iron oxide nanoparticles. J. Magn. Magn. Mater. **380**, 111–116 (2015)
21. Milkovič, O., Janák, G., Nižník, Š., Longauer, S., Frőhlich, L.: Iron nanoparticles produced by precipitation phenomena in solid state. Mater. Lett. **64**, 144–146 (2010)
22. Zak, T., Jiraskova, Y.: CONFIT: Mössbauer spectra fitting program. Surf. Interface Anal. **38**, 710–714 (2006)
23. Hammersley, A.P.: Fit2d: An introduction and overview, ESRF Internal Report, ESRF97HA02T (1997)
24. Arató, B., Szányi, Z., Flies, Ch., Schűler, D., Frankel, R.B., Buseck, P.R., Pósfai, M.: Crystal-size and shape distributions of magnetite from uncultured magnetotactic bacteria as a potential biomarker. Am. Minerol. **90**, 1233–1241 (2005)
25. Jandacka, P., Alexa, P., Pistora, J., Li, J., Vojtkova, H., Hendrych, A.: Size distributions of nanoparticles from magnetotactic bacteria as signatures of biologically controlled mineralization. Am. Minerol. **98**, 2105–2114 (2015)
26. Kohout, J., Brázda, P., Závěta, K., Kubániová, D., Kmječ, T., Kubíčková, L., Klementová, M., Šantavá, E., Lančok, A.: The magnetic transition in $\epsilon - Fe_2O_3$ nanoparticles: Magnetic properties and hyperfine interactions from Mössbauer spectroscopy. J. Appl. Phys. **117**, 17D505 (2015)
27. Zboril, R., Mashlan, M., Petridis, D.: Iron(III) oxides from thermal processes synthesis, structural and magnetic properties, Mössbauer spectroscopy characterization, and applications. Chem. Mater **14**, 969–982 (2002)
28. Shafi, K.V.P.M., Ulman, A., Dyal, A., Yan, X., Yang, N., Estournès, C., Fournès, L., Wattiaux, A., White, H., Rafailovich, M.: Magnetic enhancement of $\gamma - Fe_2O_3$ nanoparticles by sonochemical coating. Chem. Mater. **14**, 1778–1787 (2002)
29. Oh, S.J., Cook, D.C., Townsend, H.E.: Characterization of iron oxides commonly formed as corrosion products on steel. Hyperfine Interact. **112**, 59–65 (1998)
30. Hamada, M., Kamada, S., Ohtani, E., Mitsui, T., Masuda, R., Sakamaki, T., Suzuki, N., Maeda, F., Akasaka, M.: Magnetic and spin transitions in wűstite: A synchrotron Mössbauer spectroscopic study. Phys. Rev. B **93**, 155165 (2016)